Measurement of local reactive and resistive photoresponse of a superconducting microwave device

Alexander P. Zhuravel
B. Verkin Institute for Low Temperature Physics and Engineering, NAS of Ukraine, 47 Lenin Avenue, Kharkov 61103, Ukraine

Steven M. Anlage
Physics Department, Center for Superconductivity Research, University of Maryland, College Park, Maryland 20742-4111

Alexey V. Ustinov
Physics Institute III, University of Erlangen-Nuremberg, Erwin-Rommel Strasse 1, D-91058 Erlangen, Germany

We propose and demonstrate a spatial partition method for the high-frequency photoresponse of superconducting devices correlated with inductive and resistive changes in microwave impedance. Using a laser scanning microscope, we show that resistive photoresponse is mainly produced by local defects at microstrip edges and by intergrain weak links formed in the high-temperature superconducting material at the boundary between individual twin-domain blocks. These defects are known to initiate nonlinear high-frequency response. © *2006 American Institute of Physics*.
[DOI: 10.1063/1.2205726]

High-T_c superconducting (HTS) materials have been widely applied in passive high-frequency (HF) devices such as filters and resonators. Compared to their normal-metal counterparts the important advantage of superconducting (SC) devices is their small HF absorption, providing ultra-high ($>10^6$) quality factor, Q.[1] The power handling capability of HTS systems is limited by strong nonlinearity (NL) of the surface impedance in d-wave cuprates at high exciting HF field. This manifests itself as generation of spurious harmonics and intermodulation product distortion.

Despite the voluminous work on the nature of NL effects in HTS, the causes are not completely clear and remain under debate.[2] It is widely accepted that sources of this problem have both resistive and inductive origins, and arise locally as a result of high current densities $J_{rf}(x,y)$ nonuniformly distributed in the cross section of SC films. The lower limit of NLs can be attributed to the nonlinear Meissner effect (NLME), parametrized as a HF current (field) dependent magnetic penetration depth;[3,4] $\lambda_{eff}(T,J_{rf}) \cong \lambda_{eff}(T)\{1+(1/2) \times[J_{rf}(x,y)/J_{NL}(x,y)]^2\}$. Here $\lambda_{eff}(T)$ is the local value of the temperature dependent magnetic penetration depth and J_{NL} is a material parameter that corresponds to the intrinsic depairing current density in HTS. For currents above a current scale on the order of J_{NL}, penetration of vortices, hysteresis, and thermal dissipation contribute to the NL of the HTS device. Inhomogeneities generate additional resistive NL sources, with smaller values of J_{NL}, reducing the power handling capability even further. The standard methods to assess NL essentially integrate the response over the whole device[5,6] and cannot solve this problem because multiple NL sources are scattered inhomogeneously about the HTS film. Therefore it is highly desirable to develop methods of local analysis capable not only to find NL sources but also to correlate their location and effects with other properties of HTS materials, such as $J_{rf}(x,y)$ and structural perfection.

A laser scanning microscope (LSM) can measure the optical and HF properties in HTS devices simultaneously and is ideally suited for studying the above-stated problems. The LSM uses the principle of raster scanning the surface of a sample by a sharply focused laser beam (probe). The (i) reflected laser power is detected as a function of probe coordinate x,y to image optically distinguishable defects of its geometry and structure. The (ii) absorbed part of laser energy heats the sample on the thermal healing length scale l_T for bolometric probing of all the thermosensitive properties of the device, including the microwave transmittance $S_{21}(f)$. In this case, the thermally induced changes of $S_{21}(f)$ in the probe are understood as LSM photoresponse (PR) that can be expressed as $PR \propto [\partial\|S_{12}(f)\|^2/\partial T]\delta T$.

In particular, modulation of kinetic inductance by a thermal probe allows one to measure a quantity proportional to $A\lambda_{eff}^2(x,y)J_{rf}^2(x,y)\delta\lambda_{eff}$, and consequently can be used for extraction of $J_{rf}^2(x,y)$ maps.[7] Here $\delta\lambda_{eff}$ is the photoinduced change in λ_{eff}, and A is the area of the thermal spot (related to l_T). However, the local LSM bolometric PR has a more complex nature and contains a resistive component in addition to the inductive one. The amplitude of the (HF current driven) resistive LSM PR component is proportional to probe-induced dissipation in HTS and therefore also $J_{rf}^2(x,y)$. In this letter, we propose and demonstrate a way to separate resistive and inductive components of PR.

The examined sample was a coplanar waveguide (CPW) resonator designed for operation with fundamental resonant frequency of about $f_0=5.6$ GHz with $Q=600$ at a temperature of 78 K. The HTS structure was patterned by wet lithography from a YBa$_2$Cu$_3$O$_{7-\delta}$ (YBCO) film with thickness $d=240\pm28$ nm laser ablated on a 500 μm LaAlO$_3$ ($\varepsilon_r=24.2$) substrate (LAO). The CPW of $w=500$ μm width, $L_0=7.75$ mm length, and 650 μm gap from the ground plane was capacitively coupled to microwave connectors attached to a cooled Cu sample fixture. The measurements were performed in an optical cryostat stabilizing temperature of the sample between 77 K and $T_c=86.4$ K with an accuracy of 0.005 K.

The SC device was cooled below T_c and the resonant mode was excited by an external synthesizer at a frequency
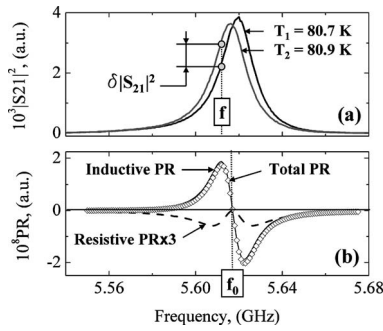
FIG. 1. (a) Microwave transmittance $|S_{21}|^2(f)$ of a CPW resonator at P_{IN} =0 dBm at two fixed temperatures T_1=80.7 K, T_2=80.9 K, with ΔT =0.2 K; (b) difference of the traces in (a) (symbols) that is proportional to the total LSM PR, along with the inductive (solid line) and resistive (dashed line) components obtained using Eqs. (1). The symmetry of the resistive component and asymmetry of the inductive component relative to f_0 is clearly visible.
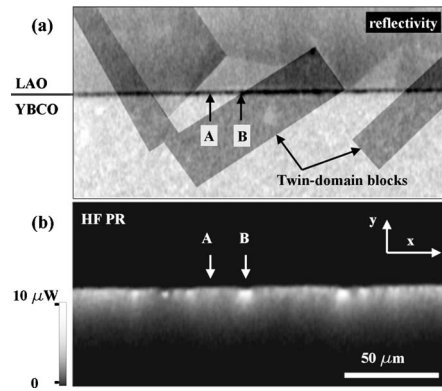

FIG. 2. (a) LSM reflectivity map showing the patterned YBCO edge and twinned structure of the LAO substrate (highlighted by dark rectangles). Total HF photoresponse in the YBCO film taken simultaneously in the same area as (a). Arrows indicate sections A and B showing a large difference in LSM PR and selected for detailed analysis. Note that the largest PR comes from points where the twin domain block edges cross the film edge.

f, producing the transmission spectrum $|S_{21}(f)|^2$ shown in Fig. 1. The surface of the CPW resonator was scanned by a laser beam (wavelength: 670 nm, power: 1 mW) focused in an optical probe of 1.2 μm diameter. The intensity of the laser is modulated with frequency $f_M=\omega_M/2\pi=100$ kHz, raising the average temperature of the sample by ΔT=0.2 K and creating a thermal probe (of $2l_T$ diameter) oscillating with magnitude $(\Delta T/2)\cos(\omega_M t+\phi)$, where ϕ is the phase shift of the temperature oscillation relative to the modulation.[8] A good acoustic match between the YBCO film and LAO substrate at temperatures above 50 K leads to an l_T that is defined mainly by the properties of LAO, producing a thermal spot with $l_T=(k/c\rho f_M)^{1/2}$=4.8 μm with thermal conductivity k=9 W/m K, a specific heat c=0.58 J/g K, and density ρ=6.57 g/cm^3. This estimate of l_T is in good agreement with the measured value.[9]

The oscillating local heating of the HTS film causes the thermoinduced modulation of transmitted HF power $\delta P_{OUT}(f)\sim\delta\|S_{21}(f)\|^2$, which was detected by a spectrum analyzer and was used as a signal of the LSM PR. The typical ratio $\delta P_{OUT}/P_{OUT}\sim10^{-6}$ depends on the ratio between the sizes of the probe and the sample. Since the variation in δP_{OUT} is on the level of HF noise, increased sensitivity is achieved by using ac lock-in detection of the spectrum analyzer signal synchronized to ω_M.

Figure 1(a) illustrates the method of extraction for the averaged properties from our data.[8] The bolometric LSM PR is modeled here with a shifting of HF transmittance $\delta\|S_{21}(f)\|^2$ of the CPW resonator by the LSM probe. In this case, the LSM PR is generated (at any fixed HF frequency f) by a jump between temperatures T_1 and T_2 corresponding to the Lorenz-like profiles of $S_{21}(f)$ characteristic of the unperturbed and perturbed resonators. The resulting (taking into account the size of the thermal probe) LSM PR is shown by symbols in Fig. 1(b). Curves T_1 and T_2 in Fig. 1(a) are the experimental $\|S_{21}(f)\|^2$ spectra of the resonator obtained at P_{IN}=0 dBm and at temperatures of 80.7 and 80.9 K, accordingly. The total $\delta\|S_{21}(f)\|^2$ has contributions from the effects of HF resonant frequency tuning δf_0 and broadening of the spectrum $\Delta f_{3\ dB}$. Generally, δf_0 is associated with the change of kinetic inductance $I_{ki}=(\mu_0/2)(l/w_s)\lambda_{eff}(T)$ due to the thermal probe, while $\Delta f_{3\ dB}\sim\Delta(1/2Q)$ is directly related to photoinduced modulation of the inverse Q factor due to an increase in local Ohmic dissipation. Their separate contribu-

tions to total LSM PR can be estimated[8] from the resonance line shape represented by $\|S_{21}(f)\|^2=S_{21}(f=f_0)/[1+4Q^2(f/f_0-1)^2]$. Using the measured temperature dependence of Q and f_0 from a set of S characteristics, the inductive PR_X and resistive PR_R components of $\delta\|S_{21}(f)\|^2$ are obtained through the partial derivatives:

$$PR_X \propto P_{IN}\frac{\partial\|S_{12}(f)\|^2}{\partial f_0}\delta f_0, \quad PR_R \propto P_{IN}\frac{\partial\|S_{12}(f)\|^2}{\partial(1/2Q)}\delta(1/2Q). \quad (1)$$

The extracted PR_R and PR_X found in this way are shown by dashed and solid lines, respectively, in Fig. 1(b). Here the symbols show the difference between curves T_2 and T_1. At this temperature PR_R is making less than a 15% contribution to the total LSM PR, and the averaged PR is generated mainly by its inductive component.

For comparison, the total local LSM PR has been measured at different areas of the CPW resonator under the same operating conditions. As an example, a 100×200 μm^2 scan is chosen in the vicinity of an edge of the YBCO center strip [see the reflective LSM image in Fig. 2(a)] close to the point of maximum $J_{rf}(x,y)$ in the standing wave pattern. The substrate clearly shows the patterns of twin domain blocks which modulate the LSM PR along the patterned edge of the YBCO film. Fig. 2(b) highlights several such blocks through dark shading. Detailed analysis of LAO twinning on the total $J_{rf}(x,y)$ was done in an earlier paper.[10] Here we are interested in elucidating the microscopic origin of the LSM PR.

Figures 3(a) and 3(b) show the frequency dependences of LSM PR in sections A and B, respectively, of Fig. 2 corresponding to the greatest contrast in $J_{rf}(x,y)$ inside the scanned area. A gray-scale representation is used for the $PR(y,f)$ LSM images, where black areas correspond to (negative) minimum of LSM PR while the brightest areas correspond to (positive) maximum response, and gray corresponds to zero. The images are acquired by repeating a 250 μm y line scan at locations A and B at different HF frequency f incremented in discrete steps of 0.1 MHz. The raster scan starts on LAO and crosses to YBCO at y=135 μm. It is clear from the marked horizontal sections of the LSM images in Figs. 3(a) and 3(b) that there is a different frequency dependence of the LSM PR at different points inside the HTS strip. As seen from Fig. 3(c), the form of the normalized (to its positive maximum) PR(f) in section A

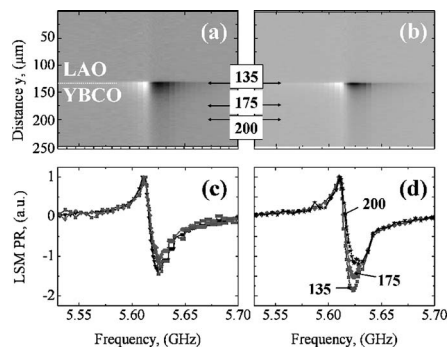FIG. 3. Gray-scale representation of frequency-dependent LSM PR taken on a 250 μm long line scan at sections (a) A and (b) B of Fig. 2 between 5.54 and 5.70 GHz. The corresponding [(c) and (d)] normalized to positive maximum amplitude frequency profiles taken at $y=135$, 175, and 200 μm showing different decays of LSM PR in the YBCO film due to the influence of twin domains.

FIG. 4. (Color online) 2D LSM images of (a) inductive PR_X and (b) resistive PR_R components of LSM PR in μV, extracted using Eqs. (2) from the data in Fig. 2.

practically remains invariant as a function of distance from the YBCO edge deep into the strip. At the same time, edge currents in section B give a sharp increase of negative LSM PR not far from the edge, showing evidence of nonlinear behavior. One possible reason for this behavior is an increase of PR_R induced by Cooper pair breaking and the generation of vortices $J_{rf}(x,y) > J_C(x,y)$ in the "weak" section B formed at the boundary of twin-domain blocks. Detailed analysis of this observation is presented elsewhere.[11]

One interesting feature is observed in the frequency dependence of the LSM PR [see Fig. 1(b)]. Its inductive component changes sign above and below f_0, where f_0 is defined as the frequency of the zero crossing of the total PR. In contrast, the resistive component is always negative and symmetrically positioned relative to f_0. This characteristic can be used for separation of the relative contribution to total PR as follows. Designate by PR($f+$) and PR($f-$) the LSM PR at equidistant frequencies $f+$ (above) and $f-$ (below) f_0, then

$$PR_R = \frac{|PR(f+) + PR(f-)|}{2}, \tag{2}$$

so that addition gives the resistive component, while subtraction gives the inductive contribution. Applying this procedure to the data in Fig. 3, the ratio $PR_X/PR_R = 0.15$ is found for section A and is in good agreement with the bolometric CPW resonator volume averaged data presented in Fig. 1. The edge HF currents in section B increase this ratio to 0.3 showing a twofold increase of resistive losses due to the changes in edge current distribution caused by substrate twinning.

A similar procedure of component partition has been applied for improved two-dimensional (2D) LSM imaging using Eqs. (1) and 2. Figure 4(a) shows the distribution $PR_X(x,y)$ along the edge of an element of the resonator from Fig. 2. The main structure of Fig. 4(a) is due to the rf current distribution $J_{rf}^2(x,y)$. The small spatial modulation of PR_X seen here is related to very small local changes in $\lambda_{eff}(T,J)$ described above. Figure 4(b) shows the distribution of $PR_R(x,y)$ in the same area of LSM scanning. The overall average magnitude of PR_R is about 4.3 times less than the
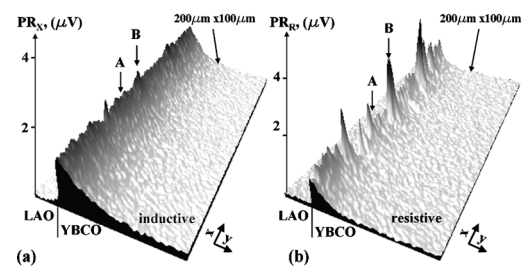
PR_X signal and is dominated by discrete features along the patterned edges. The PR_R response is highly localized and strongly fluctuating along the edge of the YBCO strip showing local maxima at the boundaries of twin-domain blocks in the substrate. Large peaks of $PR_R(x,y)$ on defects along the edge of the strip are good candidates for local sources of NL in the resonator. This interpretation is consistent with the results of Booth et al. on YBCO where they attributed resistive NL to vortex entry at the edges of their CPW transmission lines.[12]

In summary, we have developed a LSM method for a spatial partition of the HF bolometric response of HTS devices correlated with inductive and resistive changes in microwave impedance. It is shown that resistive PR is mainly produced by local defects at microstrip edges and by intergrain weak links in the HTS material arising from the underlying twin domain blocks in LAO. These defects may initiate occurrence of NL HF response due to overcritical current densities and vortex entry, and is the subject of other[11] and work.

[1] R. W. Simon, R. B. Hammond, S. J. Berkowitz, and B. A. Willemsen, Proc. IEEE **92**, 1585 (2004).
[2] S. M. Anlage, W. Hu, C. P. Vlahacos, D. Steinhauer, B. J. Feenstra, S. K. Dutta, A. Thanawalla, and F. C. Wellstood, J. Supercond. **12**, 353 (1999).
[3] G. Benz, S. Wünsch, T. A. Scherer, M. Neuhaus, and W. Jutzi, Physica C **356**, 122 (2001).
[4] D. E. Oates, S.-H. Park, and G. Koren, Phys. Rev. Lett. **93**, 197001 (2004).
[5] W. Hu, B. J. Feenstra, A. S. Thanawalla, F. C. Wellstood, and S. M. Anlage, Appl. Phys. Lett. **75**, 2824 (1999).
[6] J. C. Booth, K. Leong, S. A. Schima, J. A. Jargon, D. C. DeGroot, and R. Schwall, IEEE Trans. Appl. Supercond. **15**, 1000 (2005).
[7] J. C. Culbertson, H. S. Newman, and C. Wilker, J. Appl. Phys. **84**, 2768 (1998).
[8] M. Tsindlekht, M. Golosovsky, H. Chayet, D. Davidov, and S. Chocron, Appl. Phys. Lett. **65**, 2875 (1994).
[9] A. P. Zhuravel, A. V. Ustinov, D. Abraimov, and S. M. Anlage, IEEE Trans. Appl. Supercond. **13**, 340 (2003).
[10] A. P. Zhuravel, A. V. Ustinov, K. S. Harshavardhan, and S. M. Anlage, Appl. Phys. Lett. **81**, 4979 (2002).
[11] A. P. Zhuravel, A. G. Sivakov, O. G. Turutanov, A. N. Omelyanchouk, S. M. Anlage, and A. V. Ustinov, Low Temp. Phys. **32**, 775 (2006). cond-mat/0512582.
[12] J. C. Booth, L. R. Vale, R. H. Ono, and J. H. Claassen, J. Supercond. **14**, 65 (2001).